Engineering Structures 253 (2022) 113830

Contents lists available at ScienceDirect

Engineering Structures

journal homepage: www.elsevier.com/locate/engstruct

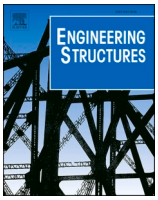

Theoretical and experimental analysis of the quasi-static and dynamic behaviour of the world's longest suspension footbridge in 2020

António Tadeu [a,c,*], António Romero [b], Filipe Bandeira [a], Filipe Pedro [a], Sara Dias [a], Miguel Serra [a], Michael Brett [a], Pedro Galvín [b,d]

[a] Itecons – Institute of Research and Technological Development in Construction, Energy, Environment and Sustainability, Rua Pedro Hispano, 3030-289 Coimbra, Portugal
[b] Escuela Técnica Superior de Ingeniería, Universidad de Sevilla, Camino de los Descubrimientos s/n, ES-41092 Sevilla, Spain
[c] ADAI-LAETA, University of Coimbra, Department of Civil Engineering, Faculty of Sciences and Technology, Pólo II, Rua Luís Reis Santos, 3030-788 Coimbra, Portugal
[d] ENGREEN, Laboratory of Engineering for Energy and Environmental Sustainability, Universidad de Sevilla, Camino de los Descubrimientos s/n, ES-41092 Sevilla, Spain

ARTICLE INFO

Keywords:
Longest suspension footbridge in 2020
Theoretical and experimental analysis
Dynamic behaviour
Nonlinear analysis
Modal identification
Damping coefficients

ABSTRACT

This work validates the simplified theoretical, analytical and numerical models used in the preliminary design stage of the 516 Arouca footbridge over the River Paiva (Portugal), the world's longest suspension footbridge. The models were used to define the configuration of the bridge under static loading and the eigenfrequencies excited under dynamic loading. The three-dimensional finite element model used in the detailed design of the bridge is briefly described.

The paper also presents in situ experimental results. Tests were performed to study the static and dynamic behaviour of the footbridge under service loads and to assess the analytical/numerical modelling assumptions. The structure was subjected to loads generated by the wind and by a group of people crossing the bridge. Global Navigation Satellite System (GNSS) antennas were used to record the displacements of the bridge under quasi-static loadings caused by the people crossing the bridge at a slow pace. The data recorded by a set of seismometers allowed us to identify the natural frequencies and modes of vibration. The agreement between all the analytical/numerical solutions and the experimental data was found to be very good. The data recorded also allowed one to evaluate the damping coefficients of the bridge for the different vibration modes, something that is very difficult to predict in the design stage.

1. Introduction

Footbridges are being designed with increasingly innovative features and different structural forms. A structural type that attracts the eye is the suspension footbridge, mainly due to its length, height, and location. In addition to serving as the link between two points, this type of bridge usually provides an exciting experience and astonishing views for pedestrians as they use it and often becomes a tourist attraction.

The 516 Arouca footbridge (Portugal) is located in the town that bears its name in the area of the Arouca Geopark, recognized as a geological heritage of international relevance, classified as a UNESCO Global Geopark. Currently, the 516 Arouca bridge is the longest suspension footbridge in the world with a span of 516 m. The bridge is in a mountainous area over the Paiva river, at a height of 175 m. In November 2020, a pilot study was conducted to evaluate the static and dynamic behaviour of the structure under pedestrian crossing loads, and some of the findings have been used in this paper.

One of the difficulties inherent in the design of pedestrian suspension bridges is the nonlinear behaviour of the cables. Different models have been proposed to take into account the nonlinear behaviour of the main cables and deck hangers [1–7].

In addition to the nonlinear behaviour, there are other difficulties in design related to the dynamic behaviour of the structure. Maraveas et al. [8] reviewed different dynamic responses of footbridges under pedestrian loads with the focus on different load models in the time domain. At the design stage, uncertainty about the predicted dynamic properties of the footbridge is inevitable [9]. Nimmen et al. [9] showed that even with the development of a detailed finite element model, deviations up

* Corresponding author at: Itecons – Institute of Research and Technological Development in Construction, Energy, Environment and Sustainability, Rua Pedro Hispano, 3030-289 Coimbra, Portugal.
E-mail address: tadeu@itecons.uc.pt (A. Tadeu).

https://doi.org/10.1016/j.engstruct.2021.113830
Received 31 August 2021; Received in revised form 16 November 2021; Accepted 29 December 2021
Available online 7 January 2022

to 10% in terms of natural frequencies can be expected. Dynamic effects on pedestrian bridges are increasingly important given the tendency to build lighter and slender structures. In addition to the action of the wind, which can lead to scenarios of resonance with vortex-induced vibrations or wind flutter [10], people crossing is another factor that can induce dynamic effects in these structures [11,12]. Pedestrians crossing the bridge produce a force with a characteristic frequency between 1.5 and 2.5 Hz for walking and jogging, and amplitude-dependent on the density of the pedestrian group [13]. Two types of synchronization mechanisms have been suggested, namely, human-to-human synchronization and human-to-structure synchronization or pedestrian lock-in. The lock-in effect is an undesirable phenomenon produced by synchronizing people's gait with the movement of the structure, leading to excessive lateral acceleration in low-damped footbridges [13,14].

The influence of several parameters on the critical number of pedestrians that trigger excessive vibrations (like the frequency of pedestrian walk steps, the sensitivity of the crowd to bridge motion, the frequency and damping), and different load conditions have been studied [15]. The walking behaviour of pedestrians during an experimental test on a footbridge is sometimes used to improve the agreement of the measured response and the simulation using a finite element model [16–18]. The vibration of slender suspension footbridges caused by eccentrically distributed dynamic walking loads has been the focus of some studies [19–21] due to the importance of torsional vibration mode shapes, which can induce a large amplitude response when they are excited.

The development of theoretical or numerical models for the dynamic analysis of this type of structure requires knowledge of natural frequencies, vibration modes, and damping factors. Although it is possible to develop numerical models to identify natural frequencies and mode shapes, structural damping can be estimated, but it is difficult to obtain reliable information until the structure has been built. This is why many footbridges undergo intervention after construction to implement control devices to mitigate the dynamic response. The Millennium Bridge in London would be the best known case [14,22]. Damping can be seen as the most important and uncertain factor that affects the response of the structure [23], as it depends on the design and materials used and the amplitude of the structural response. Typically, experimental tests are performed to estimate structural damping and validate assumptions of the design stage [23–27].

The experimental tests are based mostly on the analysis of the response produced by ambient excitation. Operational Modal Analysis (OMA) is widely used in the dynamic characterisation of structures [28–31]. Some reports discuss the application of OMA to suspension footbridges. Cunha et al. [32] discussed the importance of output-only dynamic testing to assess dynamic structural behaviour, presenting a few examples of its use in railway, road, and pedestrian bridges. Several studies experimentally identified modal parameters and dynamically characterized suspension bridges based on OMA [33–36]. Ricciardelli et al. [37] presented a study of models to study footbridge behaviour against different walking actions and concluded that design procedures should be revised and validated through full-scale data analysis.

In the design phase of the Arouca bridge, a set of simplified structural methods, including both linear and nonlinear approximations of the cables behaviour, were developed to define the initial geometrical configuration of the bridge (static analysis), displacements and the expected mode shapes and associated eigenfrequencies (dynamic analysis). The proposed formulations require less computation time and use less memory than numerical methods such as the finite element method (FEM). The use of these models is significant when defining the geometric configuration of the bridge (which also determines the tensile forces in the main cables and the natural frequencies of the in-plane and out-plane modes), which need to be applied several times to obtain the desired bridge configuration.

This work presents the design approach to enable the quasi-static and dynamic behaviour of the 516 Arouca bridge to be studied through theoretical, analytical, and numerical models. The assumptions made in these analyses are experimentally validated. The quasi-static and dynamic responses of the structure caused by wind action and people crossing were recorded by a set of GNSS antennas and triaxial accelerometers. The agreement between all the analytical/numerical solutions and the experimental data is found to be very good. The recorded data also allowed us to evaluate the damping coefficients of the bridge for the different vibration modes.

The novelties and useful contributions of the work presented herein are:

(i) The Arouca bridge is the only bridge of its kind with such a span, and therefore the presented results could be very useful for designing suspension footbridges with very big spans;
(ii) A simplified structural methodology is developed to obtain a first approximation of the static and dynamic bridge behaviour;
(iii) Simplified results are first compared in the design phase with those provided by a FEM model and later by comparing the results of in situ tests after the completion of the bridge. The numerical study includes a parametric analysis;
(iv) GNNS antennas were used to measure the static behaviour of the bridge;
(v) Experimental data on the response of this bridge, particularly on the modal damping ratios, are provided.

2. The Arouca 516 suspension footbridge

The pedestrian suspension bridge under analysis has a span of $l = 516m$ (see Fig. 1). The suspension system comprises two main cables (catenaries) and a set of secondary cables (pendants) that supports 127 metal deck modules (n_{decks}). The deck modules are connected to each other at their ends, on the same node as that where the pendants are connected.

Each module hangs from the catenaries by 8 hanger cables (shared with the adjacent modules), 4 main hangers which were designed to carry the majority of gravity loads, and 4 secondary hangers, post-tensioned, designed to minimize longitudinal deck rotation as well as a portion of lateral displacements (see Fig. 2).

The modular deck consists of segments 4.0 m long and 2.1 m wide, composed mainly of UPN profiles and a couple of angles, in S275 steel. The deck slab is formed of lightweight steel grid panels with an approximate self-weight of 25 kg/m^2. Each module has a total mass of $M = 603.2$ kg.

Catenary cables are each composed of seven 40 mm nominal diameter steel wire ropes HD 8 K PPI [38] (steel core, $A_m = 5915.0$ mm^2, and $m = 51.0$ kg/m). The ends of these cables were attached to the anchoring blocks and the cables were placed resting on a saddle at the top of the pillars, 36.3 m high. Hangers are each composed of a single 12 mm wire rope ($A_{cl} = 75.8$ mm^2 and $m_{cl} = 0.65$ kg/m). The wire ropes were previously pre-tensioned during fabrication. The Young modulus of the wire ropes was indicated by the manufacturer and experimentally verified in Itecons, with a value of $E = 100 \pm 20$ GPa. As default, the value $E = 100$ GPa was used in the computations. In addition, a parametric analysis is performed for Young modulus varying in the range $50 - 200$ GPa is performed to verify its effect. Steel plates with a hexagonal section were fitted at 4.0 m intervals on each catenary to clamp the cables and work as a connection to the secondary cables (pendants).

The configuration of the main cables and the length of the hanger cables were defined to ensure that they all remain in the same plane and lead to a maximum longitudinal inclination of the decks of 15% at the bridge ends. It was also important to guarantee that the tensile force of the main cables was very low compared to their tensile strength. After several iterations, the main cables with a length of $L_0 = 530.305$ m and a cable sag of about $d_{sag} = 53.50$ m, and secondary cables with length varying between 2.361 m and 35.684 m were defined and are used

Fig. 1. View of the 516 Arouca footbridge (Portugal).

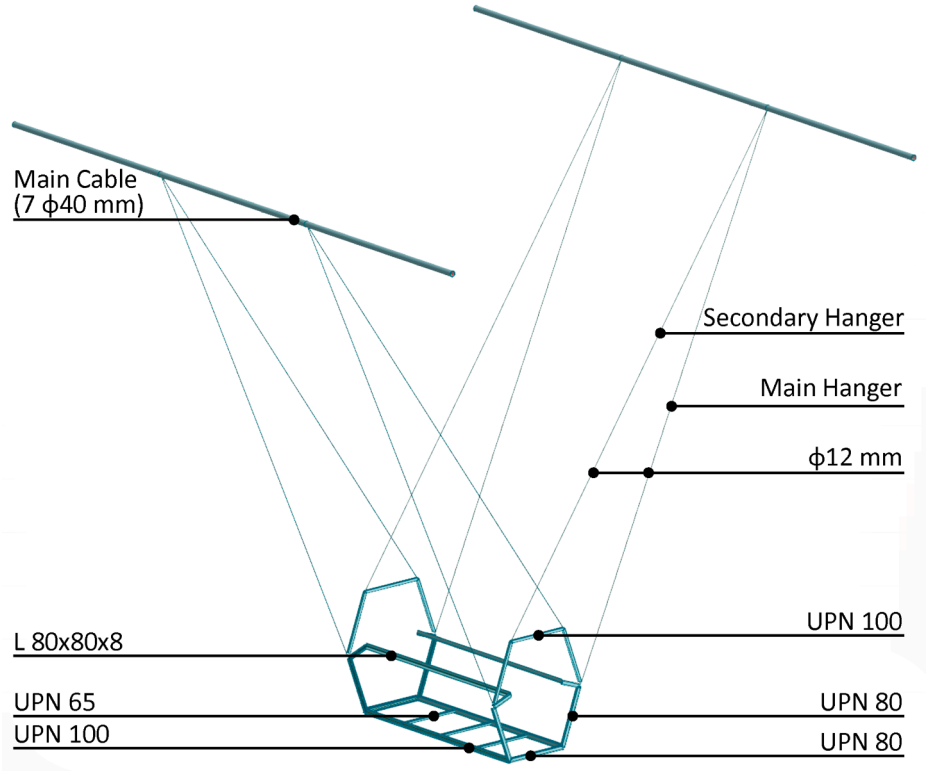

Fig. 2. Schematic of the structure module of the bridge and profiles of the construction elements.

throughout this study.

3. Theoretical analysis of the quasi-static and dynamic behaviour

This section briefly describes the analytical models used to evaluate the static and dynamic behaviour of the bridge.

3.1. Linear analysis

This subsection presents two simplified structural methods to define the initial geometrical configuration of the bridge (static analysis) and the expected mode shapes and associated eigenfrequencies (dynamic analysis). A linear behaviour was assumed for the suspended main cables. The tension in the main cables is taken to be constant along the cable, and the axial strain was neglected.

3.1.1. Static behaviour

The 2D structural scheme adopted for each of the main cables of the suspension pedestrian bridge under analysis is shown in Fig. 3. The cable tension force is assumed to be large enough to be considered constant. The axial cable stiffness is large enough for the axial strains to be neglected, and the influence of gravity forces on the cable tension variation is also neglected. So, in this phase, the deflections are assumed to be small, and the nonlinear effects will therefore be neglected when computing the in-plane mode shapes.

Defining $k = T/d$ as the stiffness of each segment of the cable, where T is the tensile force applied to the cable (assumed to be constant at this stage) and d is the distance between discrete masses, where $m_{ldi} = m(x_i - x_{i-1})$ as the mass of each cable segment between two consecutive masses, and taking M_i the mass resulting from the action of the deck boards at the end of each spring, K_i as the stiffness of each spring given by the secondary cables, and U_i the displacement of each mass placed at

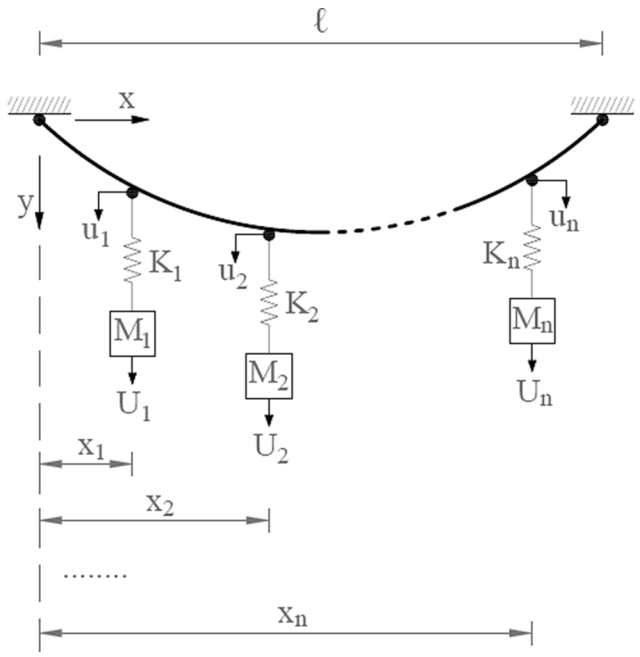

Fig. 3. Structural scheme for one of the main cables of the pedestrian suspension bridge adopted in the preliminary design stage.

the end of each spring. In this model, the springs will elongate so that at each point we will have two distinct displacements: that of the mass at the end of the spring (U_i), and another at the base of the spring where the mass is lumped to the cable segment (u_i). The masses are assumed in this preliminary design to be prevented from swinging like pendulums. As the length of each segment of the cable is constant $m_{ldi} = m_{ld}$.

The static equilibrium equations can be written as follows:

$$\begin{aligned} -(m_{ld})g + k(-u_{i-1} + 2u_i - u_{i+1}) - K_i(U_i - u_i) = 0 \\ -(M_i + m_{cli})g + K_i(U_i - u_i) = 0 \end{aligned} \tag{1}$$

with $u(0) = u(l) = 0$; $M_1 = M_n = M/4$; $M_i = M$ (for $i \neq 1$ and $i \neq n$); $K_i = \frac{EA}{C_{li}}$ (where C_{li} is the length of each secondary cable), $m_{cli} = m_{cl}\, C_{li}$ is the mass of each secondary and g is the acceleration of gravity. The tensile force T is estimated through the relation $T = \frac{m_{eq} g l^2}{8 d_{sag}}$. The equivalent mass m_{eq} combines the weight of the main cable and the weight of the decks suspended by the secondary cables (not including the secondary cables) per unit length, and l is the span of the bridge.

Then, Equation (1) can be written in the following matrix form after applying the boundary conditions:

$$\boldsymbol{K}\boldsymbol{u} = \boldsymbol{m}g \tag{2}$$

with

$$\boldsymbol{u}^T = [\,u_1 \quad u_2 \quad \cdots \quad u_n \quad U_1 \quad U_2 \quad \cdots \quad U_n\,]$$

$$\boldsymbol{m}^T = [\,m_{ld} \quad m_{ld} \quad \cdots \quad m_{ld} \quad M_1 + m_{cl1} \quad M_2 + m_{cl2} \quad \cdots \quad M_n + m_{cln}\,]$$

$$\boldsymbol{K} = \left[\begin{array}{ccccc|ccccc} 2k+K_1 & -k & & & & -K_1 & & & & \\ -k & 2k+K_2 & -k & & & & -K_2 & & & \\ & \cdots & \cdots & \cdots & & & & \cdots & & \\ & & -k & 2k+K_n & & & & & -K_n & \\ -K_1 & & & & & K_1 & & & & \\ & -K_2 & & & & & K_2 & & & \\ & & \cdots & & & & & \cdots & & \\ & & & -K_n & & & & & K_n & \end{array}\right]$$

where the dimension of $\boldsymbol{K}$ is $2n \times 2n$, with $n = n_{decks} + 1$ (number of hanger elements). Thus, each matrix element depends on the stiffness of each cable segment ($k = T/d$) and the stiffness of the secondary cables ($K_i = \frac{EA}{C_{li}}$). This model does not account for geometric nonlinearity.

The direct solution of Equation (2) gives the position of the main cable. It is important to note that modifying Young modulus of the secondary cable would not change the configuration of the main cable.

3.1.2. Dynamic behaviour

After computing the static equilibrium position, a preliminary dynamic analysis can be performed using the model illustrated in Fig. 3. The dynamic displacements are now defined as the oscillations of the mass at the end of the spring ($\overline{U}_i$), and of the base of the spring where the mass is lumped to the cable segment ($\overline{u}_i$) about the static equilibrium position. The dynamic equilibrium equations, in free vibration and neglecting the damping, can be described as follows:

$$\begin{aligned} m_{ld}\ddot{\overline{u}}_i + k(-\overline{u}_{i-1} + 2\overline{u}_i - \overline{u}_{i+1}) - K_i(\overline{U}_i - \overline{u}_i) = 0 \\ (M_i + m_{cli})\ddot{\overline{U}}_i + K_i(\overline{U}_i - \overline{u}_i) = 0 \end{aligned} \tag{3}$$

that can be written in the following matrix form:

$$\boldsymbol{M}\ddot{\overline{\boldsymbol{u}}} + \boldsymbol{K}\overline{\boldsymbol{u}} = 0 \tag{4}$$

where $\boldsymbol{M}$ is the stiffness matrix,

$$\boldsymbol{M} = \left[\begin{array}{ccc|ccc} m_{ld} & & & & & \\ & m_{ld} & & & & \\ & & \cdots & & & \\ & & m_{ld} & & & \\ \hline & & & M_1 + m_{cl1} & & \\ & & & & M_2 + m_{cl2} & \\ & & & & & \cdots \\ & & & & & M_n + m_{cln} \end{array}\right]$$

and $\overline{\boldsymbol{u}}^T = [\,\overline{u}_1 \quad \overline{u}_2 \quad \cdots \quad \overline{u}_n \quad \overline{U}_1 \quad \overline{U}_2 \quad \cdots \quad \overline{U}_n\,]$.

Defining the non-dimensional eigenvalue problem $|\boldsymbol{K} - \omega^2\boldsymbol{M}| = 0$, the eigenfrequencies and the associated modes can be determined. This model assumes that there is no increase in tension with the movement of the cable, which is absolutely correct for antisymmetric modes.

Note that if the main cable is considered to have an insignificant mass, that the hangers are very rigid, and that the mass of the decks plus the hangers is constant, the results obtained would coincide with the analytical solution given in [39]: $f_j = \frac{1}{2\pi}\sqrt{\frac{4T}{d^2 m_{eq}}}\sin\left(\frac{\pi j}{2(n_{decks}+2)}\right)$, where $n_{decks} = 127$ is the number of discrete deck modules and $d = 4$ m is the distance between discrete masses.

As mentioned above, this model assumes that the cable tension is constant along it, which does not allow for the correct evaluation of in-plane modes that generate extra tension/deformation in the cable.

3.2. Nonlinear analysis

This subsection uses a nonlinear analysis to evaluate the final geometrical configuration of the bridge for different static loads. It also computes the in-plane and out-of-plane eigenmodes. As the whole theory for this problem was derived by Irvine for suspended cables [40], only the main equations are presented.

3.2.1. Static behaviour

The following static model assumes that the main cable, with length L_0 (unstrained length), has an undetermined shape that is the length of the cable without strain in its free form. The cable length L_0 is longer than the distance between the supports D. This means that the tension of the cable varies with its position, depending on the $L_0 - D$ difference. The greater this difference, the greater the decline of the cable.

Consider that the cable is suspended between two fixed points horizontally distanced by l and a relative vertical offset of h (points with Cartesian coordinates A $(0, 0)$ and B (l,h)). The cable in its free form L_0 is greater than $D = \sqrt{l^2 + h^2}$. A point on the cable situated at a distance s from the origin, in a free state without traction, when subjected to the

own weight of the cable $W = mgL_0$ moves and occupies a new position in its strained form, described by the Cartesian coordinates x and y, and the Lagrangian coordinate p.

In the presence of suspended N discrete masses (load), the shape of the cable will be a discontinuous catenary with changes in the inclination in each point of mass. A segment of the cable (see Fig. 4) will have to obey the static equilibrium equations, along the horizontal and vertical directions. In this figure, F_i is a set of N vertical loads, T is the tension in the cable, V is the vertical reaction of the support, H is the horizontal component of the traction on the cable and s is the curvilinear abscissa.

Adopting the dimensionless relationships, $\xi = \frac{x}{L_0}$, $\eta = \frac{y}{L_0}$, $\sigma = \frac{s}{L_0}$, $\sigma_k = \frac{s_k}{L_0}$ $(k = 1, 2, ...,N)$, $\gamma = \frac{l}{L_0}$, $\tau = \frac{T}{W}$, $\chi = \frac{H}{W}$, $\phi = \frac{V}{W}$, $\psi_n = \frac{F_k}{W}$ $(k = 1, 2, ...,N)$ and $\beta = \frac{W}{EA_0}$ (A_0 is the transverse area of the not traction cable), defining $\sigma_0 = 0$, $\psi_{-1} = 0$ and $\psi_0 = 0$, using $\vartheta_n = \sum_{j=-1}^{N}\psi_j$ with $\vartheta_{-1} = 0$ and $\vartheta_0 = 0$, and imposing the boundary conditions in A and B ($x = 0$, $y = 0$, $p = 0$ in $s = 0$; $x = l$, $y = h$, $p = L$ in $s = L_0$, with L being the length of the cable in the strained form), the following equations can be derived [40]:

$$\tau(\sigma) = \sqrt{\chi^2 + (\phi - \vartheta_n - \sigma)^2} \tag{5}$$

valid for the interval $\sigma_k < \sigma < \sigma_{k+1}$ for $k = 0, 1, 2, ...,N$.

$$\xi(\sigma) = \chi\left[\begin{array}{c} \beta\sigma + sinh^{-1}\left(\frac{\phi}{\chi}\right) - sinh^{-1}\left(\frac{\phi - \vartheta_n - \sigma}{\chi}\right) \\ + \sum_{i=0}^{n}\left(sinh^{-1}\left(\frac{\phi - \vartheta_i - \sigma_i}{\chi}\right) - sinh^{-1}\left(\frac{\phi - \vartheta_{i-1} - \sigma_i}{\chi}\right)\right) \end{array}\right] \tag{6}$$

$$\eta(\sigma) = \beta\sigma\left(\phi - \frac{\sigma}{2}\right) + \sqrt{\chi^2 + \phi^2} - \sqrt{\chi^2 + (\phi - \vartheta_n - \sigma)^2} + \sum_{i=0}^{n}\left[\beta\psi_i(\sigma_i - \sigma) + \sqrt{\chi^2 + (\phi - \vartheta_i - \sigma_i)^2} - \sqrt{\chi^2 + (\phi - \vartheta_{i-1} - \sigma_i)^2}\right] \tag{7}$$

also valid for the interval $\sigma_k < \sigma < \sigma_{k+1}$ for $k = 0, 1, 2, ...,N$.

The values χ and ϕ can be obtained from the following equations,

$$\frac{\gamma}{\chi} - \beta = sinh^{-1}\left(\frac{\phi}{\chi}\right) - sinh^{-1}\left(\frac{\phi - \vartheta_N - 1}{\chi}\right) + \sum_{i=0}^{N}\left(sinh^{-1}\left(\frac{\phi - \vartheta_i - \sigma_i}{\chi}\right) - sinh^{-1}\left(\frac{\phi - \vartheta_{i-1} - \sigma_i}{\chi}\right)\right) \tag{8}$$

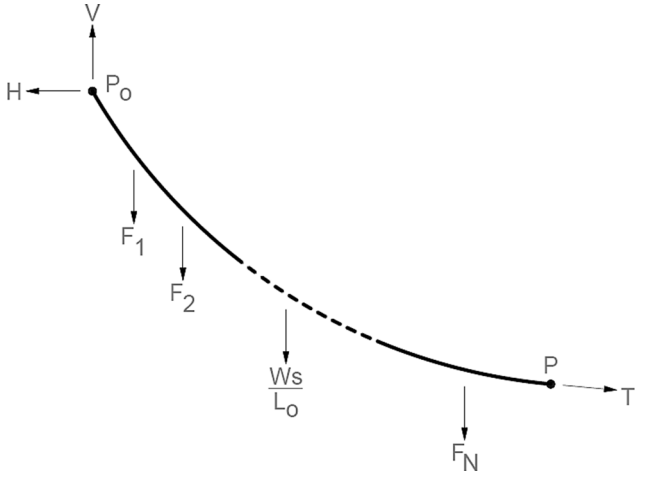

Fig. 4. Forces to which a cable segment is subjected in its equilibrium position, when submitted to N vertical hanging masses and its own weight W_s.

$$\delta = \beta\left(\phi - \frac{1}{2}\right) + \sqrt{\chi^2 + \phi^2} - \sqrt{\chi^2 + (\phi - \vartheta_N - 1)^2} + \sum_{i=0}^{N}\left[\beta\psi_i(\sigma_i - 1) + \sqrt{\chi^2 + (\phi - \vartheta_i - \sigma_i)^2} - \sqrt{\chi^2 + (\phi - \vartheta_{i-1} - \sigma_i)^2}\right] \tag{9}$$

The solution of these equations makes it possible to obtain V and H. These equations have been solved using the modified bi-dimensional Newton-Raphson method.

3.2.2. Dynamic behaviour

Disregarding the horizontal component of the motion because it is small and neglecting the second-order terms, the equilibrium equations of a suspended cable supported at the same level can be expressed by the following equations [40]:

$$T_H\frac{\partial^2\overline{u}(x,t)}{\partial x^2} + T_h\frac{\partial^2 y}{\partial x^2} - m\frac{\partial^2\overline{u}(x,t)}{\partial t^2} = 0 \tag{10}$$

$$T_H\frac{\partial^2\overline{v}(x,t)}{\partial x^2} - m\frac{\partial^2\overline{v}(x,t)}{\partial t^2} = 0 \tag{11}$$

where T_H is the horizontal component of the cable tension at the midspan, and T_h is the additional horizontal component of the cable tension. These equations correspond to the in-plane vertical $\overline{u}(x,t)$ and out-of-plane motion$\overline{v}(x,t)$, respectively.

T_h can be computed by the following integral [40]:

$$T_h = \frac{EAm_{eq}g}{T_H L_e}\int_0^l \overline{u}(x,t) \tag{12}$$

where $L_e = \int_o^l\left(\frac{ds}{dx}\right)^3 dx \approx \int_o^l l\left(1 + 8\left(\frac{d_1}{l}\right)^2\right)$ is the strained length of the cable.

In-plane motion

The in-plane motion includes antisymmetric and symmetric modes. In the presence of antisymmetric in-plane modes the additional horizontal component of the cable tension $T_h = 0$ because $\int_0^l \overline{u}(x,t) = 0$. In this specific case, Equation (11) can be written in the frequency domain after the substitution of $\overline{u}(x,t) = \widehat{\overline{u}}(x)e^{\imath\omega t}$. Knowing that $\widehat{\overline{u}}(0) = \widehat{\overline{u}}(l/2) = 0$, the following eigenfrequencies and associated eigenmodes can be computed [41]:

$$\omega_j = \frac{2j\pi}{l}\sqrt{\frac{T_H}{m_{eq}}}$$
$$\widehat{\overline{u}}_j(x) = A_j sin\left(\frac{2j\pi x}{l}\right) \tag{13}$$

where A_j is the amplitude, and $j = 1, 2, ...$

In the presence of symmetric in-plane modes, additional cable tension is induced, $T_h = \widehat{T}_h e^{\imath\omega t}$, that is taken to be constant along the span [42]. After the mathematical manipulation of Equation (10) and imposing the zero boundary conditions, the following equation is obtained:

$$\frac{T_H\widehat{\overline{u}}(x)}{m_{eq}gl^2} = \frac{\widehat{T}_h / T_H}{\overline{\omega}^2}\left(1.0 - tan\left(\frac{\overline{\omega}}{2}\right)sin\left(\overline{\omega}\frac{x}{l}\right) - cos\left(\overline{\omega}\frac{x}{l}\right)\right) \tag{14}$$

$$\overline{\omega} = \frac{\omega l}{\sqrt{\frac{T_H}{m_{eq}}}}$$

Using Equation (12) to eliminate $\widehat{T}_h / T_H$ the following transcendental equation is obtained [40]:

$$tan\left(\frac{\overline{\omega}}{2}\right) = \frac{\overline{\omega}}{2} - \frac{4.0}{\lambda^2}\left(\frac{\overline{\omega}}{2}\right)^3 \tag{15}$$

$$\lambda^2 = \left(\frac{m_{eq}gl}{T_H}\right)^2 l \Big/ \left(\frac{T_H L_e}{EA}\right)$$

The solution of Equation (15) gives the natural frequencies of the symmetric in-plane modes.

Out-of-plane motion

Assuming $\overline{v}(x,t) = \widehat{\overline{v}}(x)e^{i\omega t}$ in Equation (11), the following natural frequencies and associated modes can be computed after imposing the boundary conditions $\widehat{\overline{v}}(0) = \widehat{\overline{v}}(l) = 0$:

$$\omega_j = \frac{j\pi}{l}\sqrt{\frac{T_H}{m_{eq}}}; \quad \widehat{\overline{v}_j}(x) = B_j sin\left(\frac{j\pi x}{l}\right) \tag{16}$$

where B_j is the amplitude, and $j = 1, 2, \ldots$.

3.2.3. Cable configuration

The cable configuration is estimated from the static analysis described in the previous sections. A preliminary analysis was performed using the linear model presented in Section 3.1. The tensile force is estimated as $T = 780.2$ kN (assuming $d_{sag} = 53.00$ m) and the equivalent mass is $m_{eq} = 126.4$ kg/m. The system of Equation (1) has *256* unknown degrees of freedom (DOF). Its solution gives the initial position of the main cable, $d_{sag} = 53.50$ m (see Fig. 5a).

In addition, a nonlinear analysis allows identification of the main cable position and variation of the tensile force according to Equations (7–9). Fig. 5a and 5b show the position and the tensile force of the main cable obtained. The sag of the main cable obtained in the nonlinear analysis $d_{sag} = 53.56$ m, is similar to that given by the linear model ($d_{sag} = 53.50$ m), and the value measured in the bridge after construction ($d_{sag} = 53.72$ m). The tensile force in the cable changes from 848.1 kN at the cable ends to 781.9 kN at the midspan, higher than estimated in the linear analysis ($T = 780.2$ kN).

The result of a parametric analysis for the Young modulus varying in the range $50 - 200$ GPa shows: *i*) the sag changes from 54.83 m to 52.88 m; and *ii*) the tensile forces are in the ranges 763.1–830.9 kN ($E = 50$ GPa) and 792.1–857.6 kN ($E = 200$ GPa).

4. Numerical analysis using a finite element model

A numerical finite element model was developed in Autodesk® Robot Structural Analysis Professional software [43], using its capabilities to model cable structures subjected to large displacements, to define initial stress conditions, and to perform a modal analysis considering a stress state at the end of static analysis.

The elements forming the deck were modelled with 12DOF Euler-Bernoulli beam elements, while the cables were modelled with cable elements (tension only, 6DOF) (see Fig. 6). For load application, three nodes are added at the ends of each deck module defined by *L*, *C*, and *R*. These correspond to the theoretical centre of mass of human bodies for concentric and eccentric loads coupled with the centre of mass of the deck (see Fig. 6b). All the loads are applied to the above-mentioned points. Loads arising from self-weight and wind action are modelled as a concentrated load at point *C*. Loads arising from human activity are modelled at any of the 3 points, depending on the load case under study. The masses used in the modal analysis are equally modelled at these 3 points, with the same assumptions.

The bridge model was analysed in two steps taking into account that tension stiffening phenomena make a large contribution to its overall stiffness: 1) a nonlinear analysis to determine the shape and stress state

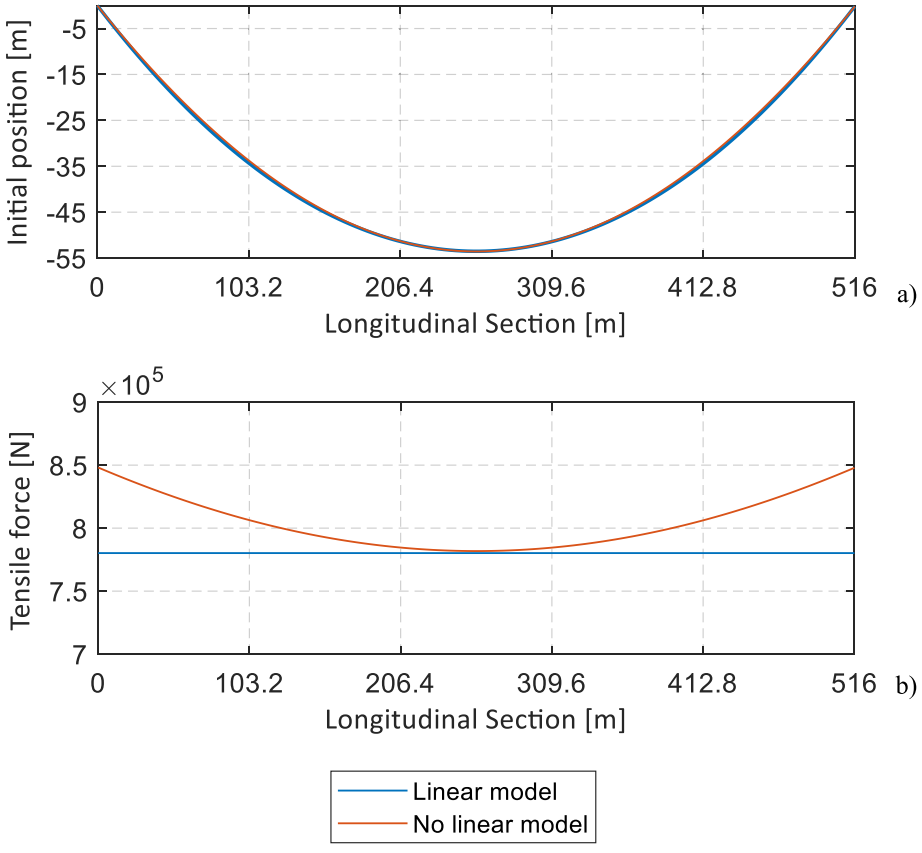

Fig. 5. Cable design obtained from the linear and nonlinear analysis: a) position; b) tensile force.

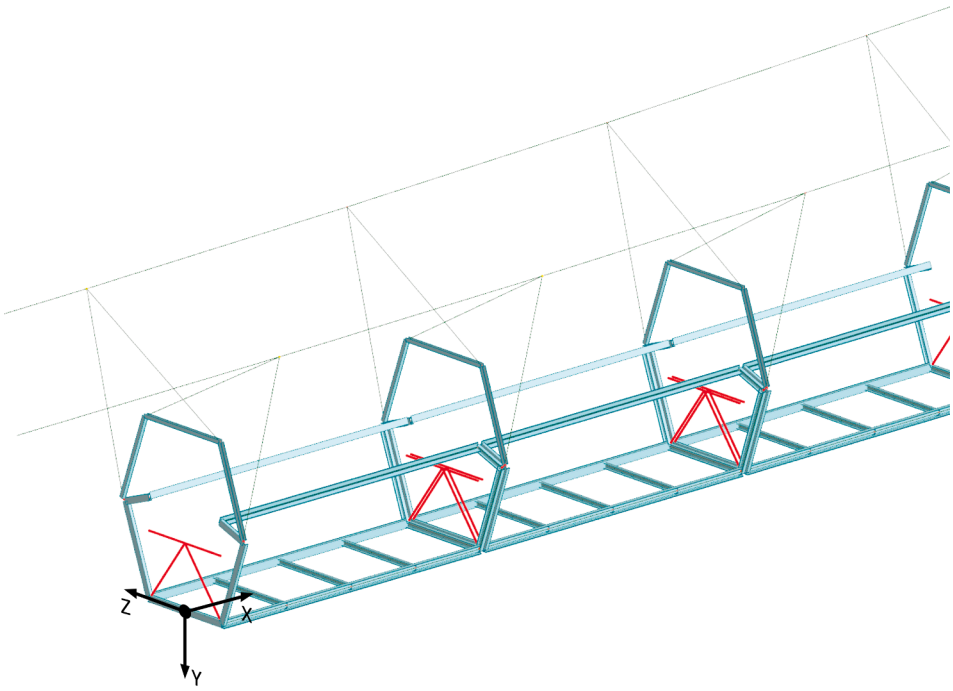

a)

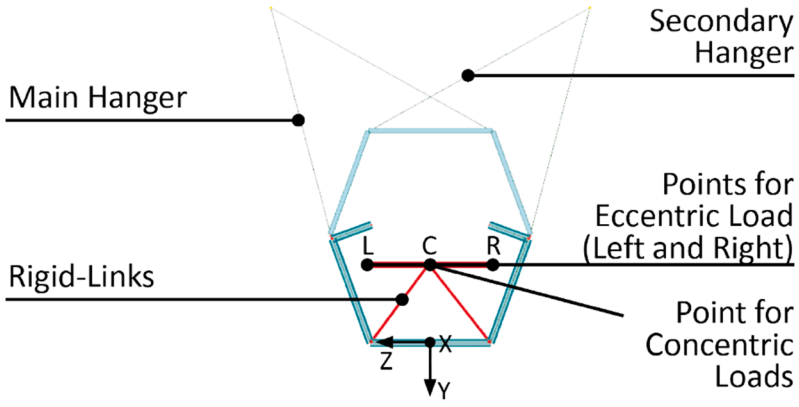

b)

Fig. 6. Partial view of the numerical model: a) longitudinal view; b) cross-sectional view.

of the structure; 2) a modal analysis using the stress state at the end of stage 1. After defining an undeformed structure, the final lengths of the catenaries upon self-weight loading and pretension levels of the hanger cables, a large displacement geometrically nonlinear analysis was carried out using a full Newton-Raphson solver. In addition to determining the final shape of the bridge under self-weight and imposed conditions, this analysis allows us to save the total stiffness and mass matrices at the end of the iterative process. The resulting stiffness matrix, also called a secant stiffness matrix, is then used as an input for the modal analysis and accounts for the extra geometric stiffness arising from tensioned elements.

5. Experimental test and results

This section presents the experimental test performed to evaluate the footbridge behaviour under service loading and identify the dynamic properties. The bridge was subjected to both a quasi-static load induced by people walking at a slow pace and the dynamic load due to the wind action. Moreover, the experimental results allow assessment of the analytical and numerical modelling assumptions.

The equipment used to evaluate the quasi-static and dynamic behaviour of *Ponte 516 Arouca* included ten triaxial accelerometers (model SYSCOM MR3000C), precision timing system clock < 1 ppm, three GNSS antennas (Leica model GS15) and an anemometer (Gill windsonic 2D) (see Fig. 7). GNNS antennas were found to be the best system for measuring the static behaviour of the bridge. Alternative

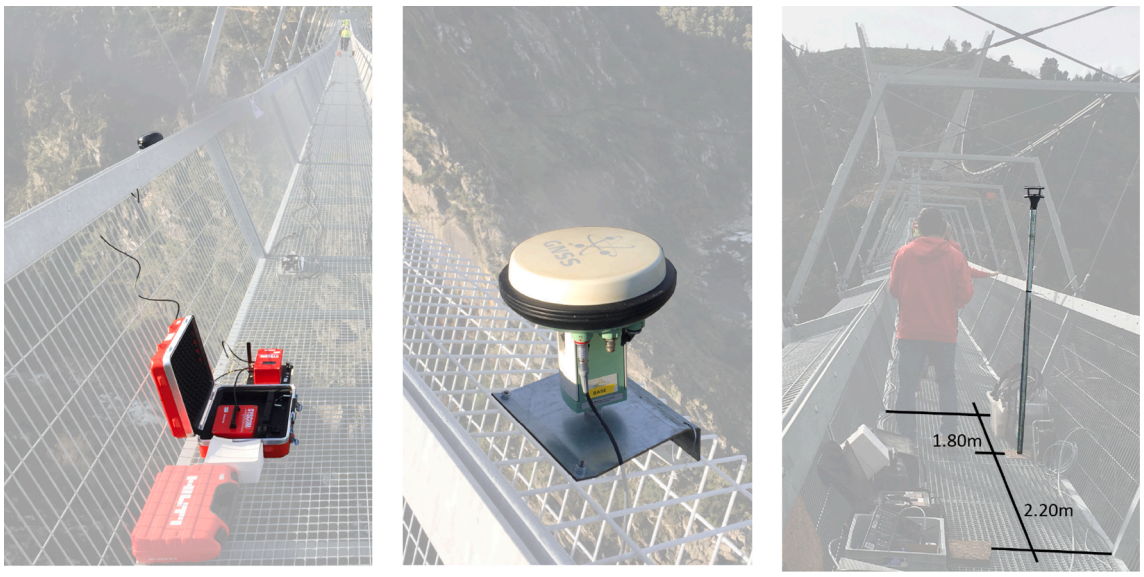

Fig. 7. Sensors used to monitor the bridge: a) Triaxial accelerometers; b) GNSS Antenna; c) anemometer.

systems, such as a displacement transducer or digital image correlation (DIC), are not available due to the characteristics of the valley. Triaxial accelerometers synchronized by GPS and wireless connectivity allowed measuring the dynamic response of the bridge at the required low frequency range. Other equipment was used, but it is not listed because it is not relevant to the content of the present paper.

The triaxial accelerometers, with a nominal sensitivity of 1.25 V/g and a frequency range from DC to 600 Hz, were distributed along the span of the bridge at the locations indicated in Fig. 8, on the upstream side of the platform. In the middle, another triaxial accelerometer was placed on the downstream side of the platform. These triaxial accelerometers provided communication with a computer via the 4G network. The equipment was operated wirelessly to reduce any electrical interference or unwanted movement produced by the operator. This communication option meant that a GPS antenna was connected to each triaxial accelerometer, thus ensuring that the internal clock of each item of equipment was synchronized. The A/D conversion was carried out at a sampling frequency, fs = 200 Hz, which avoided aliasing effects. The structural responses were filtered by applying a 50 Hz Bessel low pass filter of the 8th order to limit the analysis in the frequency range of interest 0–20 Hz.

The GNSS antennas were placed at the longitudinal coordinates $l/2$, $2\,l/3$ and $3\,l/4$. In addition to the GNSS antennas used on the bridge, a fourth antenna, designated as a reference antenna, was also placed nearby in a stable and open area (900 m away), which allowed the GNSS antennas to be used in relative mode, thus increasing their precision. This reference antenna used data from the closest reference station (Baião, 24 km away) in the National Network of Permanent Stations, ReNEP, to obtain high precision coordinates, using the PT-TM06/ETRS89 system. This reference data was then used to get the rest of the coordinates of the GNSS antennas at an acquisition rate of 20 Hz and an accuracy of 3 mm (Root Mean Square (RMS)).

The anemometer was placed at the bridge midspan. It was placed close to the middle of the deck module and above the deck platform (see Fig. 7c). It should also be noted that the porosity of the bridge modules is very high, which allows the wind speed to be measured accurately.

To perform the quasi-static test, a group of volunteers was invited to cross the bridge. The group consisted of 34 people, which is approximately a total mass of 2778 kg on the footbridge. The group crossed the bridge from the Arouca side to the Alvarenga side at a slow pace, approximately 0.5 m/s (1.8 km/h), moving along the longitudinal axis. The pace was controlled by means of a digital metronome. The people were distributed throughout the various platform modules so that no more than three people were on any module (see Fig. 9).

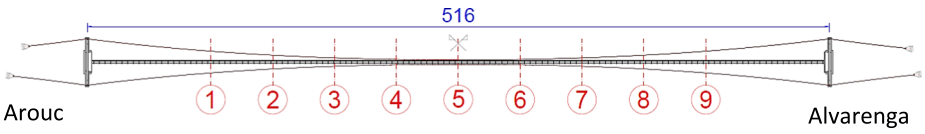

Location (Section)	1	2	3	4	5	6	7	8	9
Position relative to the span	1/6	1/4	1/3	5/12	1/2	7/12	2/3	3/4	5/6
Equipment used	a)	a)	a)	a)	a) b) c)	a)	a) c)	a) c)	a)

Fig. 8. Location of the sensors along the span of the bridge. a) Seismometer placed on the upstream side; b) Seismometer placed on the downstream side; c) GNSS antenna.

Fig. 9. The group of volunteers crossing the bridge.

5.1. Bridge response due to a quasi-static load

The loads generated by the group of volunteers were considered as discrete masses suspended on the main cables. After the mathematical manipulation of Equations (8) and (9) the displacements were computed. This nonlinear model was used to calculate the displacements

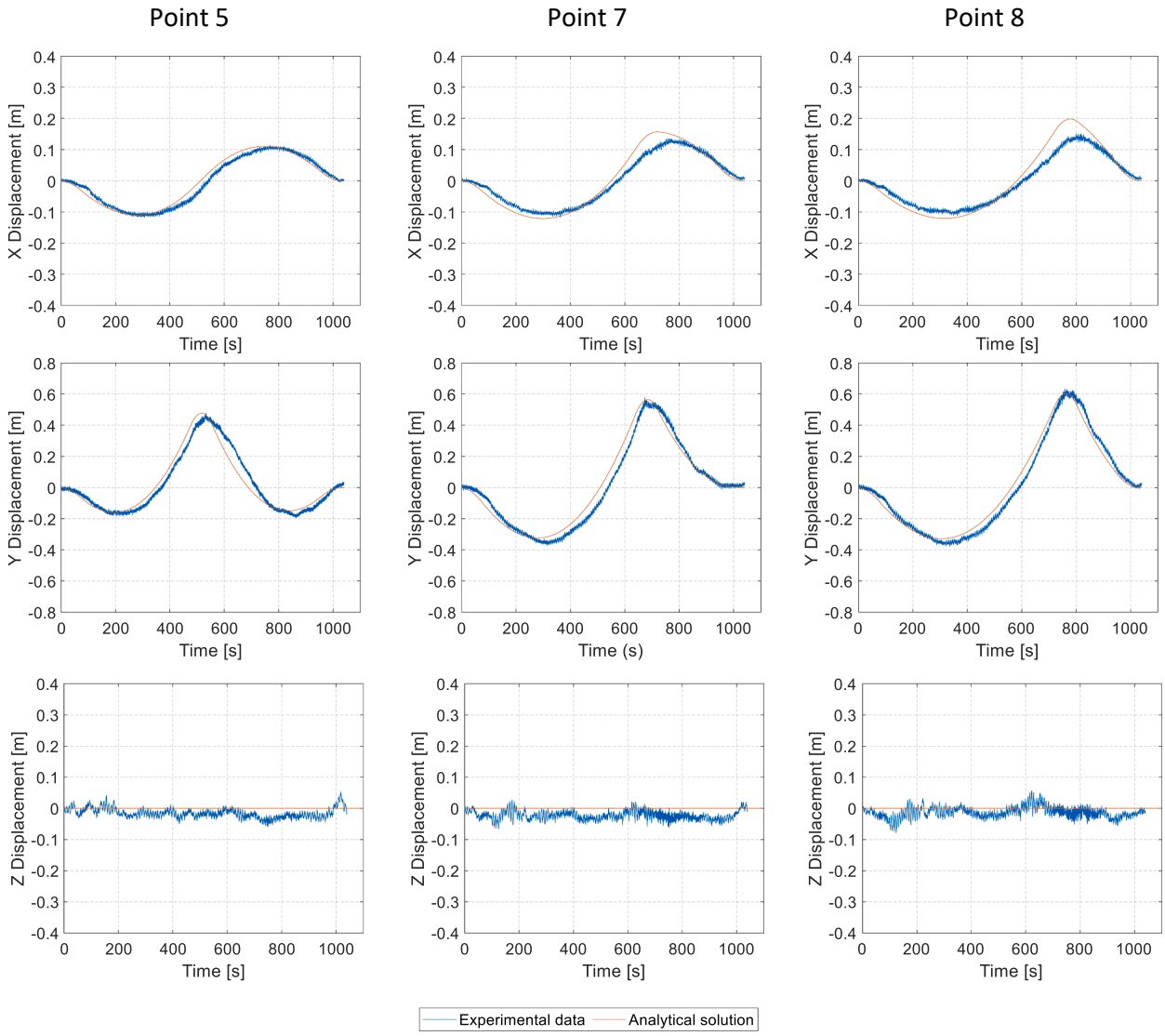

Fig. 10. Experimental displacement recorded with the GNSS antennas and analytical results at points 5, 7, and 8 due to pedestrians walking at 0.5 m/s.

obtained in three different bridge sections when the group crossed the bridge. Fig. 10 shows the computed X (longitudinal direction), Y (vertical direction), and Z (transversal direction) displacements, respectively, (assuming that the group of people is constantly distributed along 11 modules) for positions $l/2$, 2 $l/3$, and 3 $l/4$ corresponding to measurement points 5, 7 and 8 shown. These figures also include the displacements recorded by the GNSS antennas during the test.

As expected, the transversal displacement is almost zero given that the wind speed was minimal (below 3.0 m/s), and the people moved slowly. The agreement between all numerical solutions and the experimental results is very good. As can be seen, the platform modules had a maximum Y-axis displacement of 0.62 m and a maximum X-axis displacement of 0.15 m, for the three positions considered.

5.2. Modal identification

The dynamic behaviour of the structure depends on the modal parameters and excitation. Natural frequencies and modal damping ratios were identified from the structural response due to wind action. The modal parameters were found from an operational modal analysis, i.e. without knowing the input excitation, using the Enhanced Frequency Domain Decomposition (EFDD) [44]. The EFDD technique is based on the decomposition of the power spectral density of the measured acceleration using singular value decomposition (SVD). The natural frequencies of the structure are identified from the peaks of the singular values. Close to a peak, where one mode dominates, there is only one mode that contributes to the structural response, and therefore, the singular vector is an estimate of the mode shape. The corresponding singular value is the auto power spectral density function of the singular degree of freedom system which controls the structural behaviour at this frequency. This power spectral density function is identified around the peak by comparing the estimated mode shape with the singular vectors from the frequency lines around the peak. If the Modal Assurance Criterion (MAC) [45] value obtained from the singular vector, and the estimated mode shape are higher than a reference value close to one, the singular value belongs to the auto power spectral density function. Once the auto-power spectral density function has been obtained around the peak, the natural frequency and the damping ratio are estimated from the time response of the single degree of freedom system obtained by inverse fast Fourier transform.

Fig. 11 represents the SVD curves of the acceleration caused by the wind action using four projection channels and a frequency resolution of 0.0097 Hz. The singular vectors corresponding to the peaks found in the curves are estimates of the mode shapes of the structure. The experimental mode shapes are initially estimated as unit norm vectors from the OMA. Then, they are scaled using the mass normalized mode shapes obtained from the finite element model described in Section 4 [46–48].

Tables 1 and 2 summarize the natural frequencies and the modal damping ratios of the identified mode shapes represented in Figs. 12 and 13. The contribution to the structural response of frequencies up to 6 Hz has been considered. However, the number of measurement points limits the identified mode shapes. The modes that have been properly identified are discussed in the following. They were found in the frequency range below 1 Hz, and the damping ratios were between 0.35% and 1.65%. The mode shapes exhibit symmetric and antisymmetric sine forms. The lateral displacement of the upstream and downstream nodes is the same for out-of-plane mode shapes due to the stiffness of the deck.

The experimental validation of the analytical models shows that: *i*) the eigenfrequencies associated with the antisymmetric in-plane modes obtained from the linear and nonlinear models are similar (note that the antisymmetric in-plane modes do not induce additional tension T_h in the cable, which is in accordance with the condition used in Equation (3)); *ii*) the eigenfrequencies related to symmetric in-plane modes provided by the nonlinear model match the experimental results as the additional tension in the cable is considered; *iii*) for the out-of-plane mode shapes, assuming the mass m_{eq} in Equation (20), the first eigenfrequency corresponds to the lowest frequency of any given flat-sag suspended cable. However, higher discrepancies were found between the computed eigenfrequencies and the identified natural frequencies for out-of-plane mode shapes (see Table 2). This was due to the definition of an equivalent mass that considers the mass of the hangers and the secondary cables is not possible, as was done for the in-plane motion. Therefore, the analytical model cannot accurately estimate the out-of-plane mode shapes.

Tables 1 and 2 summarize, respectively, the in-plane and out-of-plane mode shapes, as well as the experimentally identified natural frequencies f_{Exp} and modal damping ratios ζ, the estimated natural frequencies given by the linear and nonlinear analytical approaches, and the numerical FE model f_{FE}, the cumulative mass fraction from the FE model, and the MAC values computed between the experimental and FE mode shapes. The relative absolute errors in relation to the experimental results are also included between brackets. The finite element model provides natural frequencies in good agreement with the experimental results, with maximum errors below 22% and 5% for in-plane and out-of-plane mode shapes, respectively. The identified mode shapes have a cumulative mass fraction of about 82% and 95% for in-plane and out-of-plane mode shapes. The MAC diagonal value is greater than 0.8 in all cases except for the sixth in-plane, and the third out-of-plane modes, probably because they were not properly excited by the wind action and the uncertainties in cable tension. The difference for the sixth symmetric

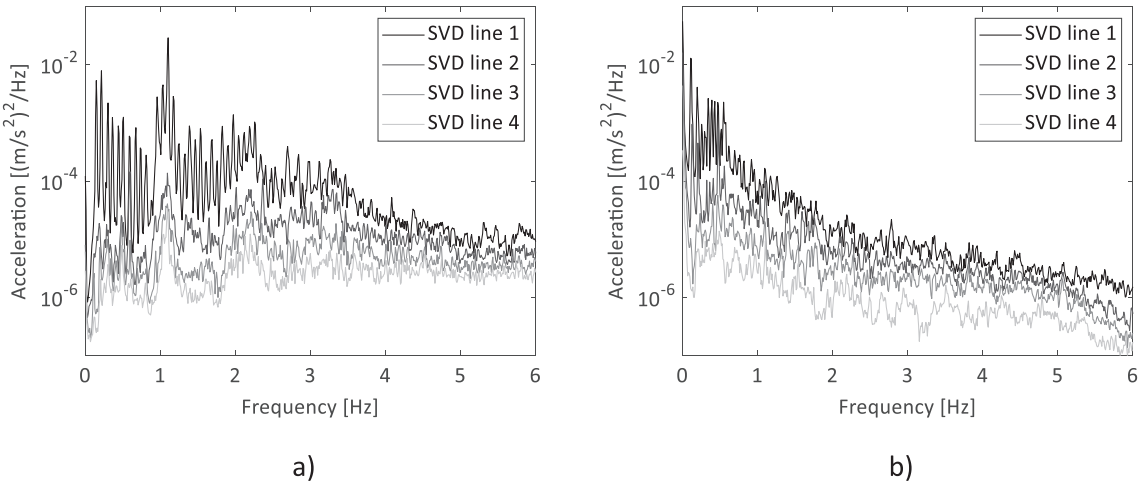

Fig. 11. Singular Value Decomposition from ambient vibration: a) in-plane mode shapes; b) out-of-plane mode shapes.

Table 1
Summary of in-plane mode shapes: estimated natural frequencies, measured modal damping ratios ζ, cumulative mass fractions from the FE model, and MAC values.

f_{Exp} [Hz]	ζ [%]	*Linear model* [Hz]	*Nonlinear model* [Hz]	f_{FE} [Hz]	Cumulative mass [%]	MAC (diagonal term) [-]
0.147	1.05	0.151 (2.7%)	0.151 (2.7%)	0.157 (6.8%)	0.0	0.999
0.214	0.70	0.226 (5.6%)	0.214 (0.0%)	0.249 (16.4%)	2.5	0.994
0.302	0.55	0.302 (0.0%)	0.303 (0.30%)	0.350 (15.9%)	2.5	0.986
0.364	0.64	0.377 (3.6%)	0.366 (0.5%)	0.418 (14.8%)	29.3	0.949
0.443	0.52	0.452 (2.0%)	0.454 (2.5%)	0.526 (18.7%)	29.3	0.975
0.504	0.57	0.526 (4.4%)	0.497 (1.4%)	0.617 (22.4%)	81.9	0.581
0.591	0.35	0.601 (1.7%)	0.605 (2.4%)	0.691 (16.9%)	81.9	0.917

Table 2
Summary of out-of-plane mode shapes: estimated natural frequencies, measured modal damping ratios ζ, cumulative mass fractions from the FE model, and MAC values.

f_{Exp} [Hz]	ζ [%]	*Linear model* [Hz]	*Nonlinear model* [Hz]	f_{FE} [Hz]	Cumulative mass [%]	MAC (diagonal term) [-]
0.113	1.45	–	0.076 (32.7%)	0.116 (2.7%)	60.2	0.951
0.131	1.65	–	0.151 (15.3%)	0.135 (3.1%)	60.2	0.853
0.196	1.48	–	0.227 (15.8%)	0.205 (4.6%)	90.6	0.585
0.214	0.84	–	0.303 (41.6%)	0.221 (3.3%)	90.6	0.979
0.257	1.65	–	0.378 (47.1%)	0.267 (3.9%)	93.2	0.966
0.293	0.91	–	0.454 (54.4%)	0.311 (6.1%)	93.2	0.973
0.344	0.95	–	0.530 (54.1%)	0.356 (3.5%)	94.8	0.945
0.389	0.90	–	0.605 (55.5%)	0.402 (3.3%)	94.8	0.953

in-plane mode is more significant because the FE model does not accurately handle the additional tension induced in the cable when this mode is excited. The MAC matrix between the experimental and FEM mode shapes is also presented in Fig. 14.

Figs. 12 and 13 show the experimental and numerical mass normalized mode shapes. Also, the analytical in-plane modes are represented in Fig. 12.

Two additional mode shapes with natural frequencies 0.407 and 0.476 Hz were identified (see Fig. 15). These mode shapes correspond to in-plane displacements with counter phase movement of points at the midspan, which produces the rotation of the deck module. Although there is only one sensor on the downstream side of the bridge, it is expected to correspond to a longitudinal torsional modes shape of the bridge. The estimated modal damping ratios are 0.914% and 0.945%, respectively.

Finally, a parametric analysis varying Young modulus in the range 50 – 200 GPa shows that the variations in the natural frequencies when computed using the nonlinear analytical model are: *i*) below 1.2% for antisymmetric in-plane modes; *ii*) between 1% and 20% for symmetric in-plane mode shapes; and *iii*) below 1.2% for out-of-plane modes. Therefore, it can be concluded that the influence of the uncertainties of the value of Young modulus on the modal parameters of the 516 Arouca suspension bridge is not very relevant.

6. Discussion

The proposed analytical linear approaches were a relevant tool in the design stage of the Arouca bridge. They allow several alternative designs to be studied and provide the results easily and quickly. These approaches assume constant tensile forces and neglect the axial strains. Therefore, the presented methodology accurately determines the position of the cable, but not the tensile force. Moreover, in-plane modes that generate extra tension/deformation in the cable, i.e. symmetrical modes, are not estimated accurately, as shown by the relative errors indicated in Table 1. The differences between the results computed by the linear model and the measurements increase for the case of symmetrical mode shapes. The differences for antisymmetric in-plane modes are lower because no additional tension is induced in the cable, and they can then be approximated by the linear model. The out-of-plane mode shapes cannot be computed by the linear approach. The results obtained from the proposed linear model agree with the analytical solution presented by Kausel [39].

The analytical non-linear approach [40] was used in the design stage to obtain the final configuration of the bridge. Its implementation is more complex, and requires more computing time than the linear approach. From this methodology, the experimental quasi-static bridge response and the in-plane (symmetric and antisymmetric) modes are accurately represented. However, the out-of-plane mode shapes computed are not representative of the actual problem since it requires the estimation of an equivalent mass for the hangers and the secondary cables, which is not well-known.

Torsional mode shapes cannot be considered by linear or nonlinear analytical models. A finite element model should be developed to handle them. The FEM model, which is used to establish the equilibrium of forces and displacement accounting for tension stiffening of the main cables, requires the implementation of a geometrically nonlinear analysis with large displacements.

The FEM analysis procedure has three stages: i) a pre-processing stage where a piecewise definition of the desired final lengths, as-built drawings, of all catenary segments and primary hangers, as well as the pre-stress levels of the secondary hangers, is provided, expected for the structure subjected to its self-weight; ii) an initial state nonlinear analysis where force equilibrium is iteratively obtained for the conditions established in the pre-processing stage; and iii) depending on the desired applied loads, a nonlinear static or time history analysis (THA) is performed, in addition to the initial state conditions, to achieve the final stress/displacement stage of the bridge subjected to external actions (live loads, wind actions). THA is also required to achieve analysis convergence for wind speeds that cause deactivation (compression) of hangers and cause momentary kinetic energy in the system. Thus, the FEM is the most time-consuming model, requiring a lot of time for preprocessing and analysis. However, it is more comprehensive. The

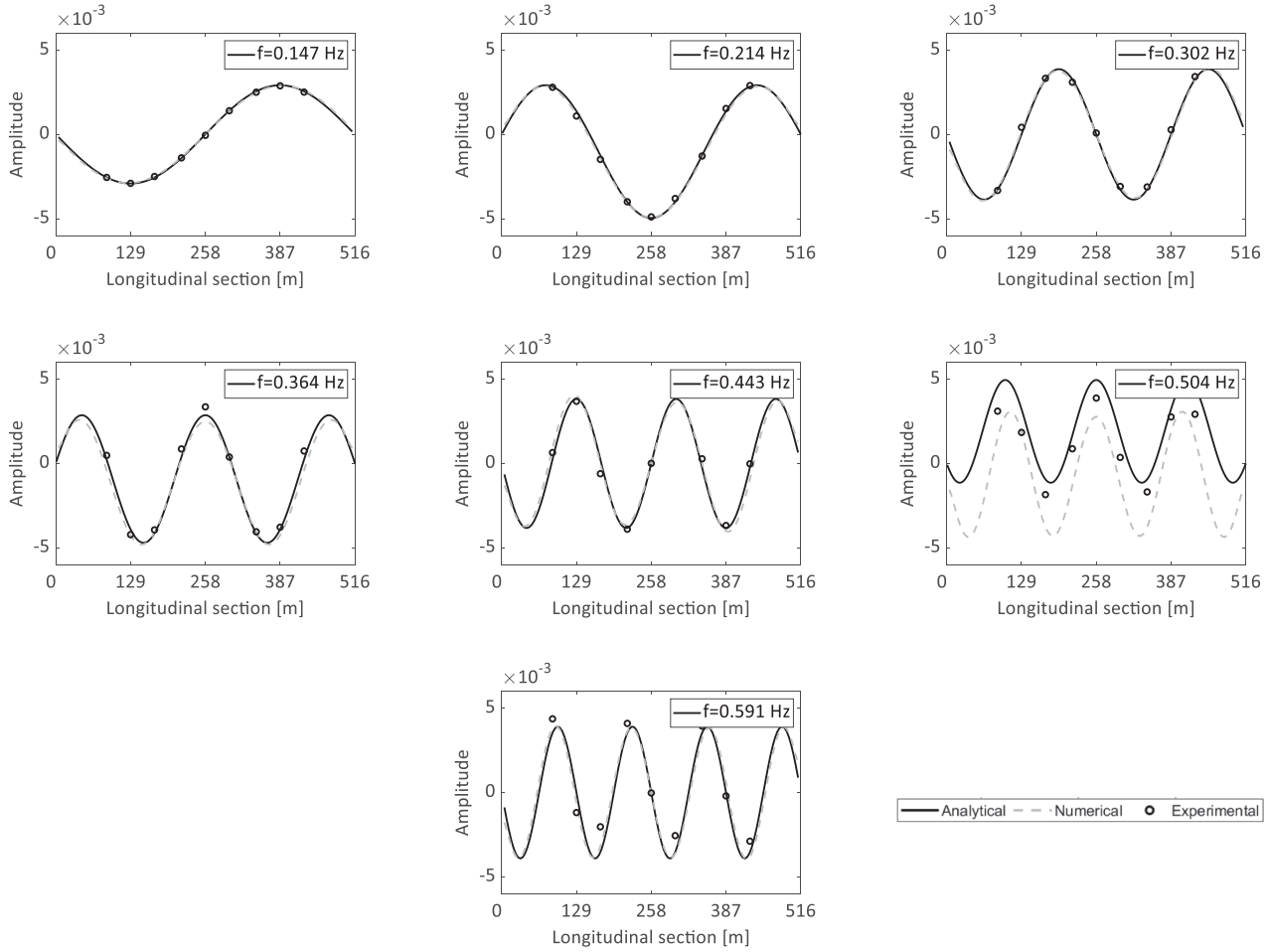

Fig. 12. Experimental, analytical and numerical in-plane mode shapes.

static and dynamic actual bridge behaviour can be accurately reproduced. The FEM allows for further dynamic study to assess the response of the bridge to pedestrian loads (not presented in this paper).

7. Conclusions

This paper illustrates an alternative simplified approach, proposed by the authors, for studying the quasi-static and dynamic behaviour of the 516 Arouca bridge using theoretical, analytical, and numerical models. The theoretical models include linear and nonlinear approximations of cable behaviour that have allowed the estimation of the static initial position and the tensile force of the bridge main cables. The main cables behave as suspended cables with an equivalent mass given by their own weight and the suspended mass of the secondary cables. The tensile force in the cable varies from 781.9 kN at the midspan to 848.1 kN in the supports.

The theoretical mode shapes and natural frequencies were obtained from the equilibrium equations of a suspended cable-supported bridge. A finite element model has also made it possible to identify of out-of-plane mode shapes. The modal analysis considered the initial deformation and the cable stress due to the self-weight of the structure.

The tests performed in situ allowed the evaluation of the behaviour of the footbridge structure under service load and assessed the numerical modelling assumptions. For this purpose, the bridge was subjected to both quasi-static and dynamic loads for different overload configurations. The analysis of the data let us: *i*) validate the numerical and analytical models used to predict the static movements; *ii*) validate the numerical and analytical models used to predict the dynamic accelerations of the bridge, essentially through the evaluation of the modal eigenvalues and eigenmodes; and *iii*) evaluate the modal damping ratios of the bridge.

The dynamic behaviour of the 516 Arouca Bridge is governed by in-plane and out-of-plane mode shapes. Frequencies below 4.0 Hz prevail in the in-plane response, and the out-of-plane behaviour occurs mainly in the frequency range below 1.0 Hz. Nevertheless, the number of measurement points has limited the identification of high order mode shapes. A total of seventeen mode shapes were properly identified in this frequency range. The estimated modal damping ratios are about 0.3–2 %. In-plane mode shapes are properly identified by both linear and nonlinear analytical models. However, the analytical model fails to predict out-of-plane mode shapes because of the difficulty of defining an equivalent mass of the hangers and the secondary cables for the lateral displacement. The FEM model accurately predicted the in-plane and out-of-plane dynamic behaviour of the bridge.

The results presented in this study have allowed the assessment of the strength of the structure and also determined the parameters needed for further analysis. The information presented will also be useful to define reference values for the bridge, which can be used for data comparison with future testing and monitoring campaigns, with the purpose of identifying possible structural alterations that may have occurred, either caused by natural deterioration of the structure or due to service load damage.

CRediT authorship contribution statement

António Tadeu: Conceptualization, Writing – review & editing,

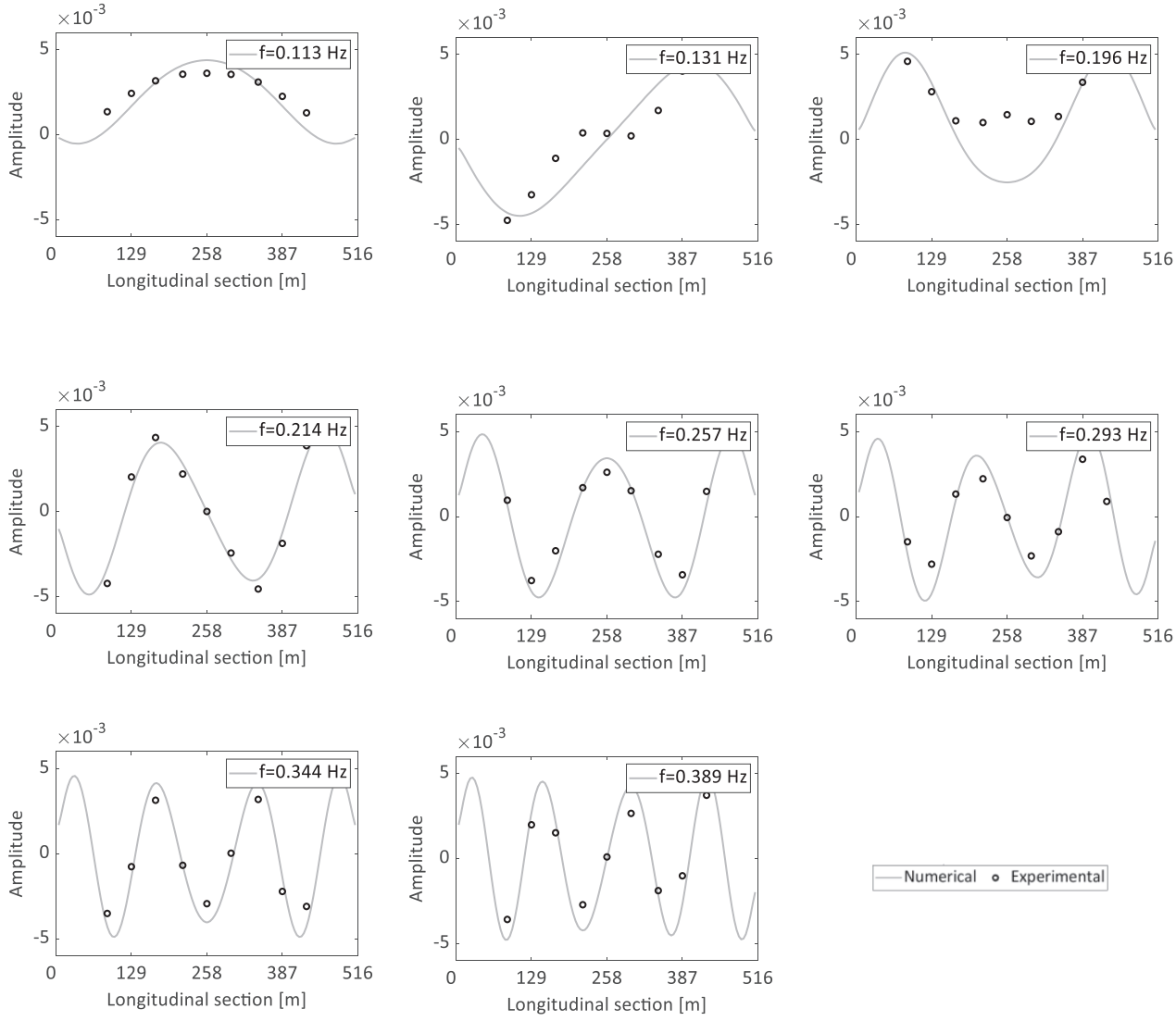

Fig. 13. Experimental and numerical out-of-plane mode shapes.

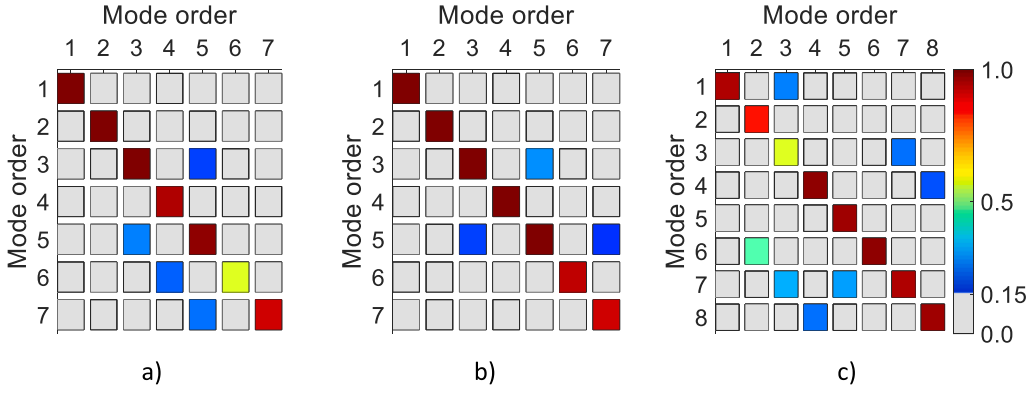

Fig. 14. MAC value between experimental and numerical results: a) in-plane from FEM; b) in-plane from nonlinear analytical approach; c) out-of-plane from FEM.

Methodology, Investigation, Supervision. **António Romero:** Writing – review & editing, Software, Investigation, Methodology. **Filipe Bandeira:** Conceptualization. **Filipe Pedro:** Validation. **Sara Dias:** Writing – review & editing. **Miguel Serra:** Software. **Michael Brett:** Validation. **Pedro Galvin:** Writing – review & editing, Software, Investigation, Methodology.

Declaration of Competing Interest

The authors declare that they have no known competing financial

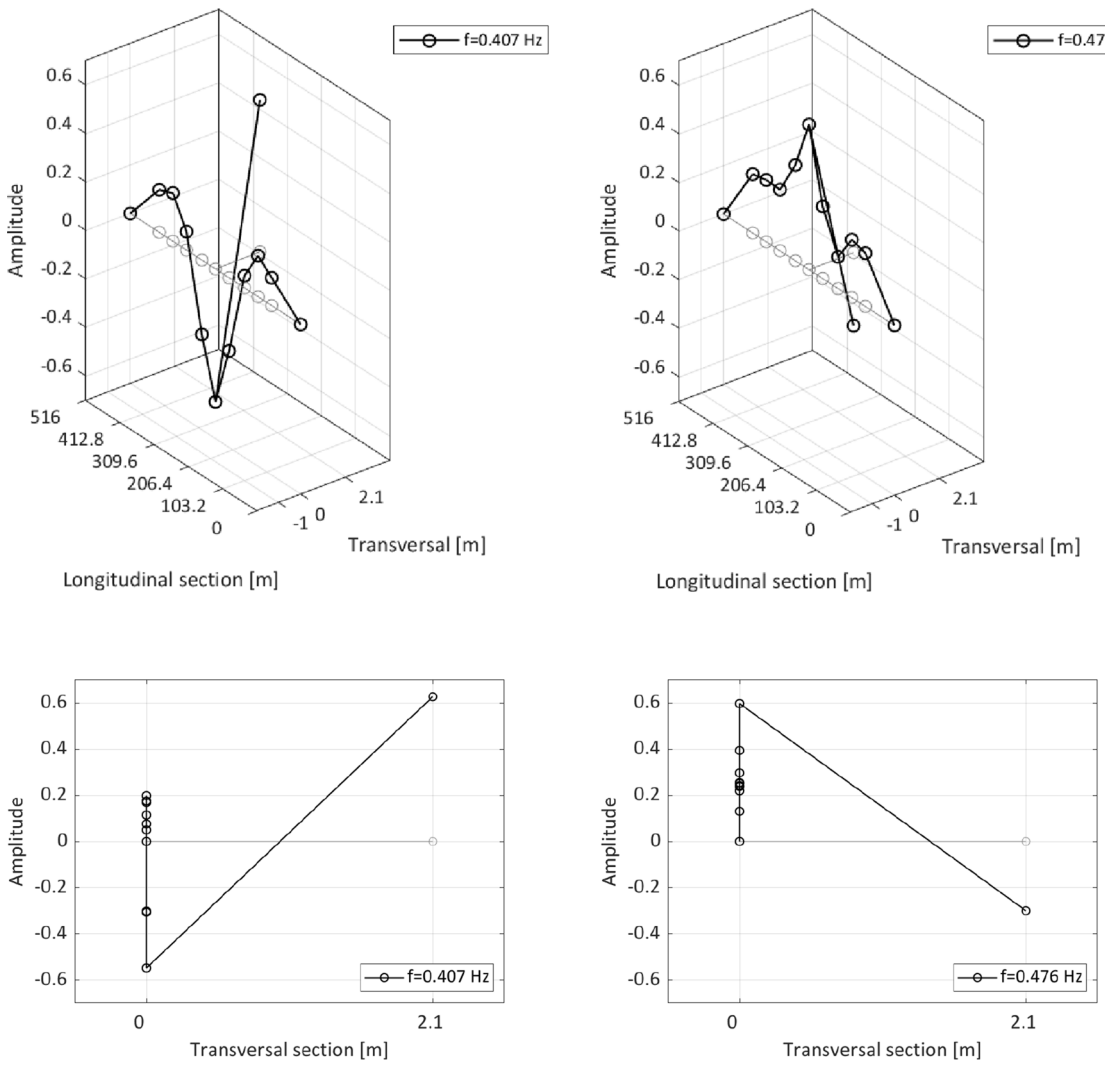

Fig. 15. Experimental torsional mode shapes (black) and the undeformed structure (grey).

interests or personal relationships that could have appeared to influence the work reported in this paper.

Acknowledgements

The authors would like to acknowledge the support provided by Arouca City Hall (Câmara Municipal de Arouca), with special gratitude to the President, Margarida Belém, and the Council Engineer, Conceição Oliveira; to the group of 34 volunteers for their time and patience; to the Portuguese enterprises MEO - Serviços de Comunicações e Multimédia, S.A and Geoide Geosystems SA, for the internet connection and GNSS antennas data, respectively; to LNEC (National Laboratory of Civil Engineering) for the anemometer data and their help in coordinating the group and the work; to Prof. Eduardo Kausel From MIT for his help with defining the analytical models. Finally, the authors would also like to acknowledge the financial support provided by the Spanish Ministry Science, Innovation and University (PID2019-109622RB-C21), and by the FEDER Andalucía 2014-2020 Operational Program (US-126491).

References

[1] Schlaich M, Brownlie K, Cozett J, Sobrino J, Stráský J, Takenouchi K. fib Bulletin 32: Guidelines for the design of footbridges 2005.
[2] Malík J. Generalized nonlinear models of suspension bridges. J Math Anal Appl 2006;324(2):1288–96.
[3] Bruno L, Venuti F, Scotti A. Limit of hanger linearity in suspension footbridge dynamics: A new section model. J Sound Vib 2011;330(26):6387–406.
[4] Bruno L, Venuti F, Nascé V. Pedestrian-induced torsional vibrations of suspended footbridges: Proposal and evaluation of vibration countermeasures. Eng Struct 2012;36:228–38.
[5] Chen Z, Cao H, Zhu H, Hu J, Li S. A simplified structural mechanics model for cable-truss footbridges and its implications for preliminary design. Eng Struct 2014;68:121–33.
[6] Lepidi M, Gattulli V. A parametric multi-body section model for modal interactions of cable-supported bridges. J Sound Vib 2014;333(19):4579–96.
[7] Lepidi M, Gattulli V. Non-linear interactions in the flexible multi-body dynamics of cable-supported bridge cross-sections. Int J Non Linear Mech 2016;80:14–28.
[8] Maraveas C, Fasoulakis ZC, Tsavdaridis KD. A Review of Human Induced Vibrations on Footbridges. American J. Eng. Appl. Sci. 2015;8(4):422–33.
[9] Van Nimmen K, Lombaert G, De Roeck G, Van den Broeck P. Vibration serviceability of footbridges: Evaluation of the current codes of practice. Eng Struct 2014;59:448–61.
[10] Li H, Laima S, Zhang Q, Li Na, Liu Z. Field monitoring and validation of vortex induced vibrations of a long-span suspension bridge. J Wind Eng Ind Aerodyn 2014;124:54–67.
[11] Ingólfsson ET, Georgakis CT, Jönsson J. Pedestrian-induced lateral vibrations of footbridges: A literature review. Eng Struct 2012;45:21–52.
[12] Venuti F, Bruno L. Crowd-structure interaction in lively footbridges under synchronous lateral excitation: a literature review. Phys Life Rev 2009;6(3):176–206.
[13] Bertram JEA, Ruina ANDY. Multiple walking speed–frequency relations are predicted by constrained optimization. J Theor Biol 2001;209(4):445–53.
[14] Dallard P, Fitzpatrick AJ, Flint A, Le Bourva S, Low A, Ridsdill Smith RM, et al. The London Millennium Footbridge. Structural Engineer 2001;79(22):17–33.
[15] Han H, Zhou D, Ji T, Zhang J. Modelling of lateral forces generated by pedestrians walking across footbridges. Appl Math Model 2021;89:1775–91.

[16] Van Nimmen K, Lombaert G, Jonkers I, De Roeck G, Van den Broeck P. Characterisation of walking loads by 3D inertial motion tracking. J Sound Vib 2014;333(20):5212–26.
[17] Shahabpoor E, Pavic A, Racic V. Structural vibration serviceability: New design framework featuring human-structure interaction. Eng Struct 2017;136:295–311.
[18] Brownjohn JMW. Vibration characteristics of a suspension footbridge. J Sound Vib 1997;202(1):29–46.
[19] Huang M-H, Thambiratnam DP, Perera NJ. Dynamic performance of slender suspension footbridges under eccentric walking dynamic loads. J Sound Vib 2007;303(1-2):239–54.
[20] Roberts TM. Lateral pedestrian excitation of footbridges. J Bridge Eng 2005;10(1):107–12.
[21] Piccardo G, Tubino F. Parametric resonance of flexible footbridges under crowd-induced lateral excitation. J Sound Vib 2008;311(1-2):353–71.
[22] Macdonald JHG. Lateral excitation of bridges by balancing pedestrians. Proc Roy Soc A 2009;465(2104):1055–73.
[23] Živanović S, Pavic A, Reynolds P. Vibration serviceability of footbridges under human-induced excitation: a literature review. J Sound Vib 2005;279(1-2):1–74.
[24] Racic V, Pavic A, Brownjohn JMW. Experimental identification and analytical modelling of human walking forces: literature review. J Sound Vib 2009;326(1-2):1–49.
[25] Hoorpah W, Flamand O, Cespedes X. The Simon de Beauvoir footbridge in Paris - Experimental verification of the dynamic behaviour under pedestrian loads and discussion of corrective modifications. Proceedings of Footbridge 2008. Porto: third international conference; 2008.
[26] Butz C, Dist J, Huber P. Effectiveness of horizontal tuned mass dampers exemplified at the footbridge in Coimbra. Porto: third international conference; 2008.
[27] Bachmann H. Case studies of structures with man-induced vibrations. J Struct Eng 1992;118(3):631–47.
[28] Brownjohn JMW, Fok P, Roche M, Omenzetter P. Long span steel pedestrian bridge at Singapore Changi Airport —part 2: Crowd loading tests and vibration mitigation measures. Structural Engineer 2004;82(16):28–34.
[29] Brincker R, Zhang LM, Andersen P. Modal identification from output-only systems using frequency domain decomposition. Smart Mater Struct 2001;10:441–5.
[30] Van Overschee P, De Moor B. Subspace Identification for Linear Systems. Boston, MA: Springer US; 1996.
[31] Galvín P, Domínguez J. Dynamic analysis of a cable-stayed deck steel arch bridge. J Constr Steel Res 2007;63(8):1024–35.
[32] Cunha Á, Caetano E, Magalhães F. Output-only dynamic testing of bridges and special structures. Struct Concr 2007;8(2):67–85.
[33] Araújo MC, Brito HMBF, Pimentel RL. Experimental evaluation of synchronisation in footbridges due to crowd density. Struct Eng Int: J Int Assoc Bridge Struct Eng (IABSE) 2009;19(3):298–303.
[34] Caetano E, Cunha Á, Magalhães F, Moutinho C. Studies for controlling human-induced vibration of the Pedro e Inês footbridge, Portugal. Part 1: Assessment of dynamic behaviour. Eng Struct 2010;32(4):1069–81.
[35] Lai E, Gentile C, Mulas MG. Experimental and numerical serviceability assessment of a steel suspension footbridge. J Constr Steel Res 2017;132:16–28.
[36] Bedon C. Diagnostic analysis and dynamic identification of a glass suspension footbridge via on-site vibration experiments and FE numerical modelling. Compos Struct 2019;216:366–78.
[37] Ricciardelli F, Demartino C. Design of Footbridges against Pedestrian-Induced Vibrations. J Bridge Eng 2016;21(8). https://doi.org/10.1061/(ASCE)BE.1943-5592.0000825.
[38] https://www.oliveirasa.com/Portals/0/Documents/Product-Specs/hd8k.pdf, consulted on 23 of August of 2021.
[39] Kausel E. Advanced Structural Dynamics. Cambridge University Press; 2017.
[40] Max IH. Cable structures. Cambridge, Mass: MIT Press; 1981.
[41] Rega G. Nonlinear vibrations of suspended cables, Part I: Modeling and analysis. Appl Mech Rev 2004;57(6):443–78.
[42] Luongo A, Rega G, Vestroni F. (1984), Planar non-linear free vibrations of an elastic cable. Int J Non Linear Mech 1984;19(1):39–52.
[43] Autodesk Robot Structural Analysis Professional, Autodesk 2020.
[44] Brincker R, Zhang L, Andersen P. Modal identification of output-only systems using frequency domain decomposition. Smart Mater Struct 2001;10(3):441–5.
[45] Allemang RJ, Brown DL. Correlation coefficient for modal vector analysis. In: Proceedings of International Modal Analysis I, Orlando (8-10 November 1982), pp. 110-116.
[46] Aenlle ML, Brincker R. (2013) Modal scaling in operational modal analysis using a finite element model. Int J Mech Sci 2013;76:86–101. https://doi.org/10.1016/j.ijmecsci.2013.09.003.
[47] Aenlle ML, Brincker R. Modal Scaling in OMA Using the Mass matrix of a Finite Element Model. Dynamics Civil Struct. 2014;4:263–70. https://doi.org/10.1007/978-3-319-04546-7_30.
[48] Pelayo F, Aenlle ML, Brincker R. Mass normalization of a 3D tubular structure combining operational modal analysis and a numerical model. Proceedings of ISMA 2014 International Conference on Noise and Vibration Engineering, USD 2014 International Conference on Uncertainty in Structural Dynamics 2014.